J Mater Sci (2018) 53:4540–4553

Energy materials

Impact of position and number of nitrogen atom substitution on the curvature and hydrogen adsorption properties of metallized borophene

Azin Shahsavar[1] and Afshan Mohajeri[1,*]

[1] Department of Chemistry, College of Sciences, Shiraz University, Shiraz, Iran

Received: 23 August 2017
Accepted: 6 December 2017
Published online: 11 December 2017

ABSTRACT

Motivated by experimental observation of B_{36} borophene as a molecular model of bulk boron, here, we report the impact of nitrogen substitution on the electronic and chemical properties of neutral and anionic B_{36} clusters. Three N-doped configurations resulted from nitrogen substitution at different positions with respect to the central hexagonal hole of B_{36} are considered. The effect of N-doping on the structure, curvature, and π bonding pattern of the B_{36} is analyzed. High level of N-dopant enhances the curvature, and the cluster adopts a buckled form. We also study the binding strength between alkali metals with the pristine and N-doped substrates. Moreover, the adsorption properties of metallized substrates toward H_2 molecule are explored, highlighting the role of dopant. Depending on the type of metal and the nitrogen content, the H_2 adsorption energies vary in the range between -0.11 and -0.21 eV which fall into the range for the practical applications.

Introduction

Superexcellent properties of boron nanostructures have been led these wonder materials in the center of attention [1–5]. Boron nanostructures have the same merit as carbon nanomaterials such as lightweight, extreme hardness, and porous [6, 7]. Recently, a new two-dimensional boron sheet, borophene, has been synthesized on the Ag(111) substrates [8]. The exploration of borophene offers a broad perspective in medicine, material research, catalysis, and photonic devices [9]. Furthermore, the quasi-planar structure, low atomic weight, and high stability of borophene make it an attractive potential choice for the energy storage and conversion systems [10–13]. Over the past decade, combined experimental and theoretical studies have led to a systematic understanding of the structural and bonding properties of small boron clusters [14, 15]. Recently, a quasi-planar boron cluster, B_{36}, with a central hexagonal vacancy and sixfold symmetry has been synthesized by Piazza and coworkers [16]. This B_{36} cluster represents a record size for freestanding quasi-planar atomic clusters and is an embryo for the formation of extended two-dimensional boron sheets [6, 7, 17]. The unique structure of B_{36} with a natural hole is capable

Address correspondence to E-mail: amohajeri@shirazu.ac.ir

https://doi.org/10.1007/s10853-017-1900-1

of lots of applications. For example, Rastgu et al. [18] investigated the reactivity and electronic sensitivity of B_{36} borophene toward four nucleobases of adenine, guanine, thymine, and cytosine. Their results suggest a new method for determination of DNA sequencing by use of B_{36}. In a recent study, the potential application of B_{36} as a sensor for detecting toxic gases such as formaldehyde has been demonstrated [19]. Increasing research interests in B_{36} have encouraged scientists to explore further beneficial methods for energy generation prospects [20–25]. It is known that metallization of nanostructures is an efficient and industrial way to develop forefront of energy-related materials. Although alkali metals [26, 27], alkaline earth metals [28, 29], and transition metals [30, 31] are extensively investigated in this case, lighter metal adatoms can help to achieve higher gravimetric density [32]. On the other side, there are many literature studies indicating that B doping on carbon nanostructure can enhance storage capacity in metal ion batteries, decreases diffusion barrier, and raises metal reversible storage [33, 34]. Therefore, it is expected that pure boron or boron-rich materials achieve great performance as an electrode in rechargeable ion batteries. The adsorption and diffusion of commercial metal ions on freestanding borophene have received great research interest in recent years [35]. Experimental and theoretical studies indicate that borophene can serve as an ideal electrode material with high electrochemical performance for both Li-ion and Na-ion batteries [22, 24].

The advantage of borophene over carbon nanostructures and the experimental observation of B_{36} give us an impetus to examine it as a possible hydrogen storage material. Liu et al. [6] showed that Li adsorbed on neutral and anionic B_{36} can serve as reversible hydrogen storage media. Nonetheless, for efficient and economic H_2 operation (adsorption/desorption) the optimal binding energy between hydrogen molecule and the host should be 0.1–0.3 eV/H_2 [36]. To cover downside of the weak interaction between H_2 molecules and the host, chemical modifications and decoration with foreign metal are successful techniques [37]. Accordingly, in the current contribution, we study the effect of local nitrogen doping on the structure, electronic, and adsorption properties of B_{36} and its anion. Our main concerns are as follows: (1) How does the local position of dopant affect the structure and the curvature of the B_{36} cluster? (2) How do the electronic structures of pristine and doped B_{36} change after decoration with light alkali metals (Li, Na, K). Does the binding strength between metal and the B_{36} clusters depend on the concentration and location of nitrogen dopant? (3) How do the B/N content and the metal affect the adsorption behaviors of metallized N-doped B_{36} toward H_2 molecule?

Computational methods

All structures were fully relaxed by density functional theory (DFT) calculations at PBE0/6-31G* level. The PBE0 was lately benchmarked as a reliable DFT method for the boron system [17, 38, 39]. Further, Romanescu et al. [40] performed an UV–IR double-resonance experiment to obtain absorption spectra of boron clusters. They also calculated IR spectra of the three low-lying isomers of B_{11}, B_{16}, and B_{17} in the wavelength range of 650–1550 cm^{-1} using different DFT methods. The best agreement between experimental IR spectrum and calculated IR was observed for PBE0 method. Accordingly, all structural optimization and electronic surfaces analyses in the present study were accomplished by PBE0 as implemented in GAUSSIAN 09 package [41].

In order to have criteria for structural stability of the clusters, the formation energy is calculated as follows:

$$E_{\text{form}} = (E_{\text{cluster}} - n_{\text{N}}E_{\text{N}} - n_{\text{B}}E_{\text{B}})/n_{\text{tot}} \quad (1)$$

where E_{cluster} is the total energy of the cluster, E_{N} is the energy of a nitrogen atom in N_2 molecule, E_{B} is the energy of an isolated boron atom, and n_{N}, n_{B}, and n_{tot} represent the number of nitrogen, boron, and total atoms in the cluster, respectively.

The binding strength between metal (M = Li, Na, and K) and boron cluster is obtained from the expression, $E_{\text{b}} = E_{\text{M/cluster}} - E_{\text{M}} - E_{\text{cluster}}$, in terms of the energy of an isolated metal E_{M}, and the energy of boron cluster with and without metal adatom ($E_{\text{M/cluster}}$ and E_{cluster}). Also to evaluate adsorption behavior of metallized substrates toward single hydrogen molecule, the adsorption energy is calculated by:

$$E_{\text{ads}} = E_{\text{H}_2-\text{M/cluster}} - E_{\text{M/cluster}} - E_{\text{H}_2} \quad (2)$$

$E_{\text{H}_2-\text{M/cluster}}$ denotes the total energy of a hydrogen molecule adsorbed on metallized substrate and E_{H_2} is the energy of an isolated hydrogen molecule. Apart from energetic criteria, for all systems under our

consideration, including pristine, metallized, and hydrogen adsorbing systems, the harmonic vibrational frequencies were calculated to affirm that the obtained structures are true minima. Bonding analyses were performed using the adaptive natural density partitioning (AdNDP) approach [42]. The AdNDP patterns, the deformation maps of electron density, and the topological analysis of the electron localization function (ELF) were performed with MultiWFN program [43, 44].

Results and discussion

Nitrogen doping

Structure and energetics of N-doped borophene

Both B_{36} and its anion are quasi-planar with the shape of a bowl having a central hexagonal vacancy [16]. B_{36} encircles three different sizes of rings as shown in Fig. 1. Inner, middle, and outer rings each contain 6, 12, and 18 boron atoms, respectively. The N-doped analogous of the B_{36} cluster can be designed by replacing B–B unit by B–N in each ring. We consider three doped clusters by introducing three, six, or nine nitrogen atoms into the inner, middle, and outer rings of B_{36} resulting into formation of $B_{33}N_3$, $B_{30}N_6$, and $B_{27}N_9$ clusters (Fig. 1). All the atomic coordinates of doped clusters were fully relaxed during the geometry optimization without symmetry constraints. To screen the perturbation effect of N-doping on the structure and curvature of B_{36}, we consider three structural parameters including the height of bowl, the length of the cluster, and the diameter of a sphere fitted inside of cluster cavity. The detailed structural information is given in Table S1 in Supplementary Material. As shown in Fig. 1, doping at the inner ring has little effect on the cluster geometry and $B_{33}N_3$ retains its bowl shape. The bowl height becomes (1.56 Å) which is larger than that of B_{36} (1.17 Å), but the cluster length remains almost unchanged. On the contrary, B_{36} undergoes great structural deformation upon N-doping at the middle and outer rings. In $B_{30}N_6$, substitution six boron atoms at the middle ring with six nitrogens result in a cone-like structure with the height of 3.65 Å. Also in $B_{27}N_9$ the bowl transfigures to a disordered geometry having the height and the length of 4.01 Å and 7.33 Å, respectively. The bond length between B and N is 1.28–1.50 Å which is smaller than the distance between two B atoms (1.58–1.74 Å). Consequently, the cluster undergoes compression upon N-doping. In $B_{33}N_3$, the core cavity becomes slightly smaller than that of all-boron B_{36}. Moreover, $B_{33}N_3$ has six additional pentagonal vacancies around the central pore. In the case of $B_{30}N_6$, some boron atoms move above the nominal ring and some move below that caused buckling. Deformation around the inner and middle rings shrinks the central cavity and produces several larger vacancies at the bottom of the cone. In $B_{27}N_9$, the nitrogen dopants have farther distance from the central vacancy and the compression occurs mostly at the cluster length. Thus, $B_{27}N_9$ has the largest central cavity that may be helpful for its application as an adsorbent. It should also be noted that the structures of N-doped B_{36}^- clusters are similar to those of neutral B_{36} with small geometry change (see Supplementary Material for detailed structural parameters).

In addition to the structure, the thermodynamic and kinetic stability of the doped systems is also crucial for application purpose. The feasibility of N-substitutions in the borophene is assessed through the formation energy using Eq. (1). The negative values of formation energies indicate that the N-doped borophenes are energetically stable although their surfaces are no longer quasi-planar and prefer to buckle. The variation of formation energies is presented in Fig. 2. For both neutral and anion, the formation energy decreases by increasing the impurity concentration, indicating a decrease in the thermodynamic stability of the N-doped clusters as compared to the all-boron structure. On the other hand, a standard way of evaluating the stability of such molecular systems is to study the energy separation between the highest occupied molecular orbital (HOMO) and lowest unoccupied molecular orbital (LUMO). The higher HOMO–LUMO gap (E_g) is an indicator of a more stable system with less chemical reactivity. The HOMO–LUMO gaps of B_{36} and B_{36}^- are 1.22 and 1.18 eV. Interestingly, we see an opposite trend for the variation of E_g in the neutral and anionic clusters (Fig. 3). The N-doping at the inner and middle rings of the neutral B_{36} lowers the HOMO–LUMO gap, while doping at the outer ring raises the E_g. In the case of anionic clusters, the trend is quietly reversed. However, it is worthy to note that in all N-doped

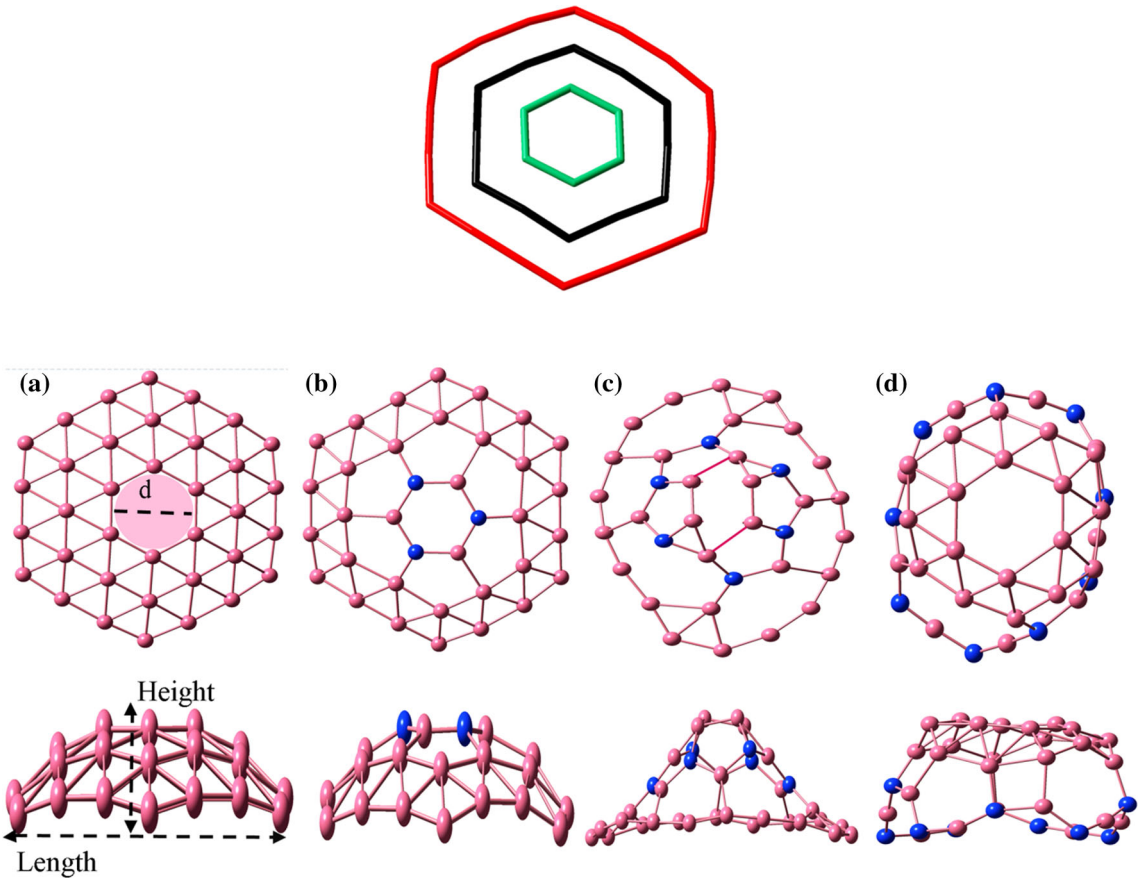

Figure 1 Illustration of three concentric rings in B_{36}: inner ring (green), middle ring (black), and outer ring (red). Top and side views of **a** B_{36}, **b** $B_{33}N_3$, **c** $B_{30}N_6$, **d** $B_{27}N_9$. The height, the length, and the cavity size are also shown in B_{36}.

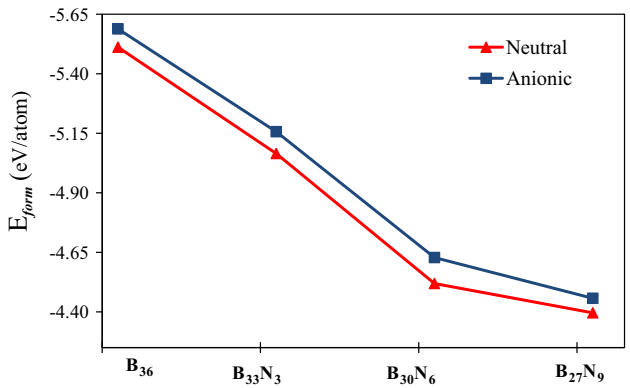

Figure 2 Formation energy of pristine and N-doped B_{36} clusters.

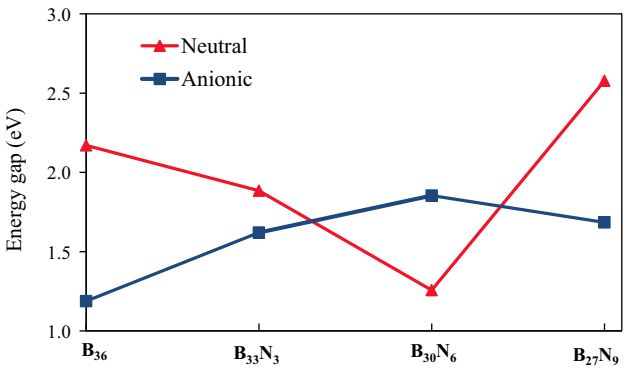

Figure 3 The energy gaps of pristine and N-doped B_{36} clusters.

B_{36}^- clusters, the gaps are greater than that of the pure undoped cluster.

To identify the effect of N-doping on the electronic structure of boron clusters, we have plotted total density of states (TDOS) for considered systems (Fig. 4). Comparing the TDOS of the original B_{36} cluster (solid line) with N-doped clusters (dashed line) reveals the appearance of new peaks in the vicinity of Fermi energy which in turn implies the strong hybridization between nitrogen and boron atoms. The N-doping at the inner and middle rings shifts the Fermi level to lower energies and induces the *p*-type behavior. Moreover, we also present the spin-polarized DOS plots of anionic clusters in Fig. S1 in Supplementary Material. The asymmetric

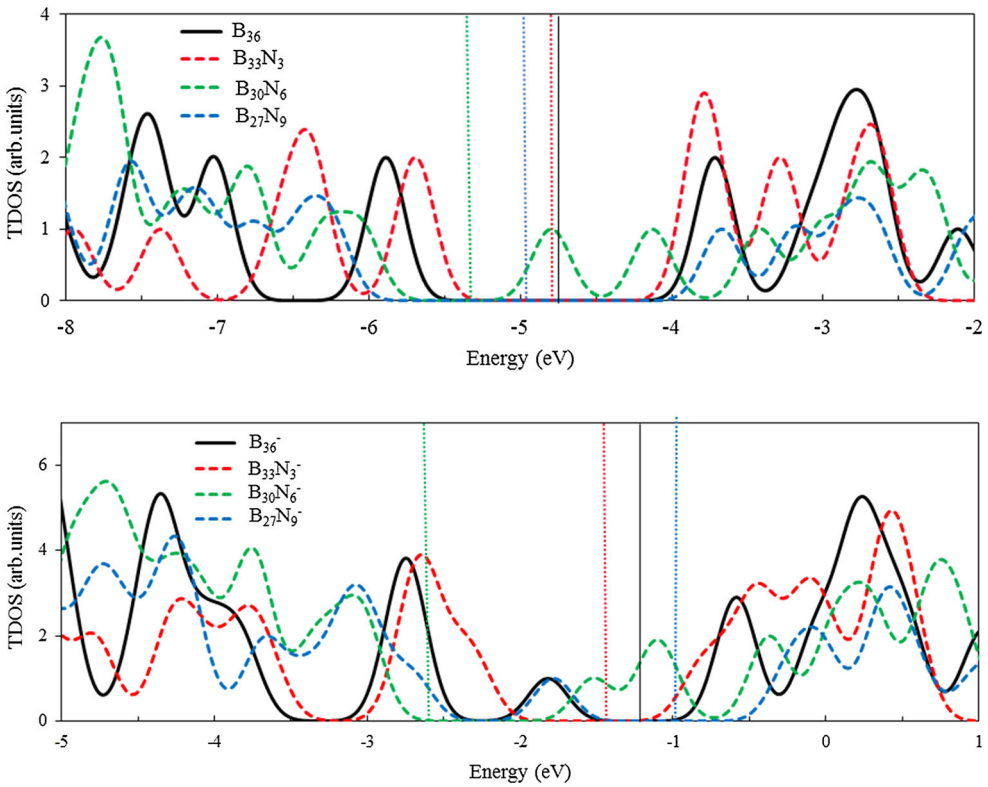

Figure 4 TDOS plots of pristine and N-doped B_{36} clusters. Fermi energies are shown by vertical lines.

behaviors of up and down spins near the Fermi level result in a nonzero magnetization in B_{36}^- and its N-doped structures.

Chemical bonding analysis: adaptive natural density partitioning

To understand more details on the bonding properties of considered doped systems, we performed AdNDP analysis. AdNDP has been introduced as a bridge between canonical molecular orbitals (CMOs) and natural bond orbitals (NBOs). CMOs are highly delocalized; meanwhile, NBOs are appreciably localized. AdNDP is an extension of NBO analysis featuring both localized and delocalized bonding without invoking the concept of resonance. In AdNDP analysis, density matrix has been localized by *n*-center two electron orbitals (*n*c-2e) with *n* spanning the interval from one to the total number of atoms in the system. However, there is no unique rule on how to search orbitals and pick out candidate orbitals as AdNDP orbitals. Actually, some molecules may have more than one reasonable AdNDP patterns. In this context, different AdNDP patterns have already been proposed for B_{36} [16, 45]. Herein, we just focus on the AdNDP results for the π bonding frameworks. To be specific, comparisons of the π orbitals between the inner rings of B_{36} and $B_{33}N_3$ (6c-2e), the middle rings of B_{36} and $B_{30}N_6$ (12c-2e), and the outer rings of B_{36} and $B_{27}N_9$ (18c-2e) are made (Figs. 5, 6, 7). Earlier studies indicate that B_{36} and B_{36}^- are all-boron analogs of coronene ($C_{24}H_{12}$) featuring concentric dual π aromaticity [45, 46]. Accordingly, we also performed AdNDP analysis for coronene and its doped derivatives ($C_{21}N_3H_{12}$ and $C_{15}N_9H_6$) resulted from nitrogen substitution at the inner and outer ring, respectively. The AdNDP patterns of π bonding in the inner rings of B_{36} and $B_{33}N_3$, as well as $C_{24}H_{12}$ and $C_{21}N_3H_{12}$, are presented in Fig. 5a–d. Interestingly, similar bonding patterns are observed not only for B_{36} and $C_{24}H_{12}$ but also for the doped structures $B_{33}N_3$ and $C_{21}N_3H_{12}$, demonstrating the close analogy between the π bonds in the $B_{33}N_3$ and $C_{21}N_3H_{12}$. In Figs. 6 and 7, we proposed two new optimal π orbitals in middle and outer rings with acceptable occupation numbers (ON). In a previous study, Chen et al. [45] demonstrated a one-to-one correspondence between 2c-2e, 4c-2e, and 6c-2e π bonds of B_{36} with those of $C_{24}H_{12}$. Here, such correspondence has also been observed for 6c-2e and 18c-2e π orbitals of borophene and coronene. More interestingly, our AdNDP analysis for the doped

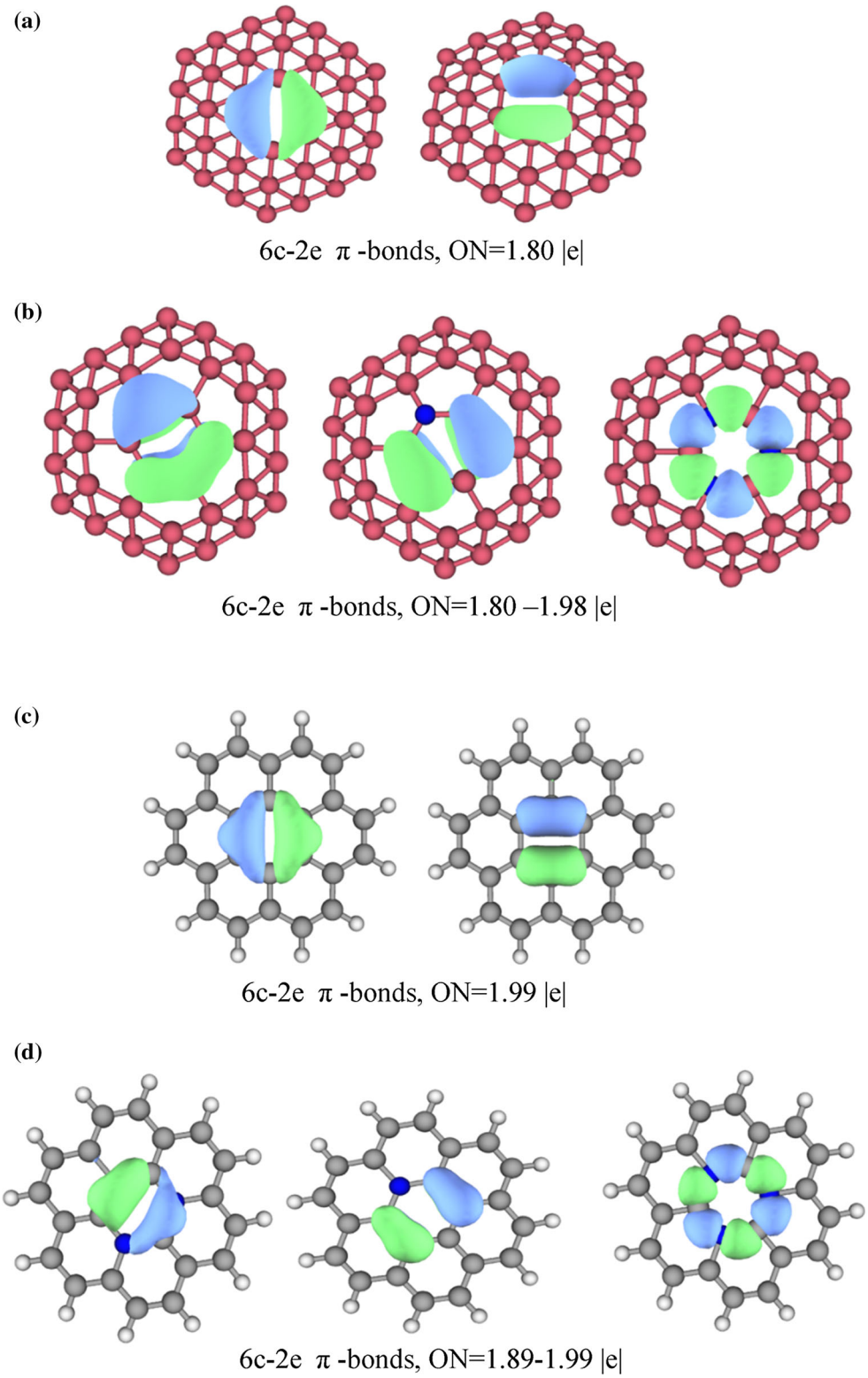

Figure 5 π bonding analysis using the AdNDP method for inner ring in **a** B_{36}, **b** $B_{33}N_3$, **c** $C_{24}H_{12}$, **d** $C_{21}N_3H_{12}$. The occupation numbers (ONs) are indicated.

clusters indicates the same analogy between π bonding patterns of N-doped coronene and N-doped borophene.

Electron density deformation upon N-doping

To achieve a deep insight into the redistribution of electron density upon N-doping, the electron density

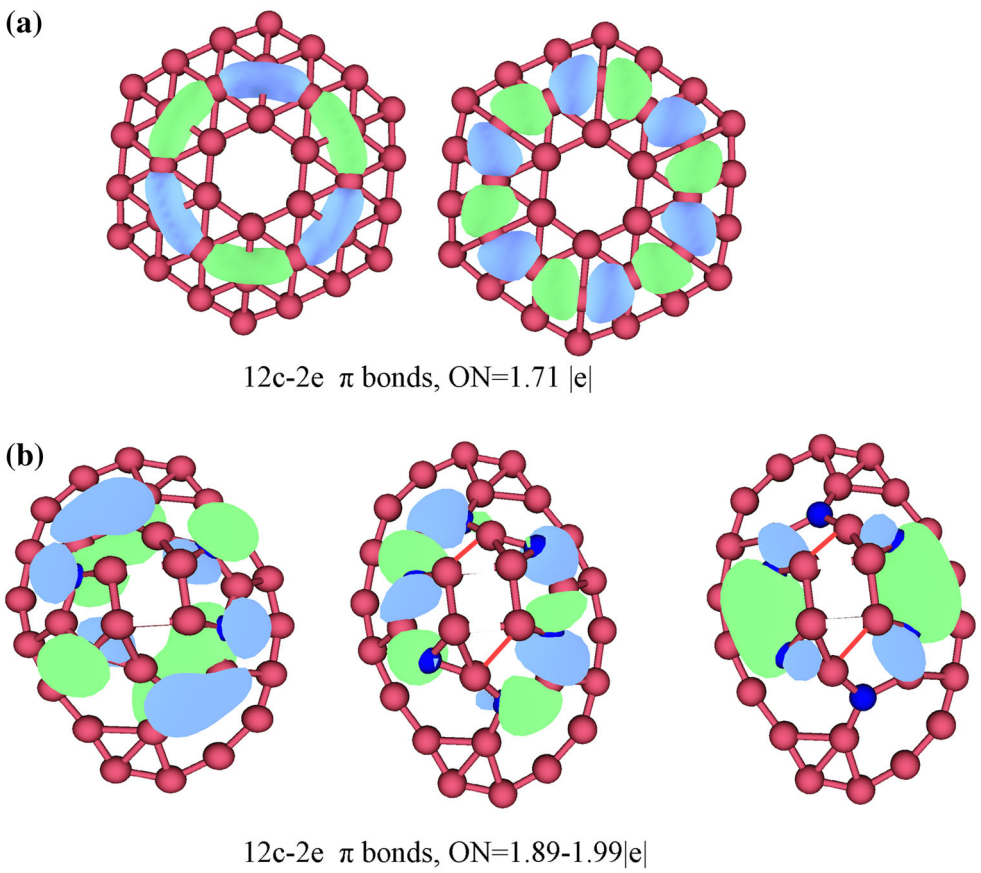

Figure 6 π bonding analysis using the AdNDP method for middle ring in **a** B_{36} and **b** $B_{30}N_6$.

deformation is adapted. Deformation densities can be generated to visualize the difference between the total electron density of the molecule and the superimposed densities of the constituent non-interacting atoms. Graphical representation of the deformation density maps is shown in Fig. 8. The blue and red lines represent the positive and negative density differences which arise from charge density accumulation and depletion, respectively. Evidently, in B_{36} regions of positive deformation density indicate the formation of covalent bonds between boron atoms of an individual ring and boron atoms belonging to two neighboring rings (Fig. 8a). N-doping at the inner ring does not lead to significant change into the distribution of electron density around the middle and outer rings (Fig. 8b). Nonetheless, the map shows that extra electrons of the N-dopant stay locally on nitrogen and weaken the bonds in the inner ring. In the nitrogen-rich structures, the symmetric bonding pattern is lost (Fig. 8c, d) and the depletion of electron density leads to an anisotropic distribution of electron density over the whole $B_{30}N_6$ and $B_{27}N_9$ clusters. Thus, although B_{36} itself is a highly stable cluster, however, it cannot bear introducing the dopant.

Metallization

To understand the effect of N-doping and charge state of the substrate on the alkali metal binding properties, we first calculate the binding energy between Li atom and B_{36} cluster. Different initial adsorption sites of Li on B_{36} are considered, including above the convex and concave sides of the central hexagonal cavity, triangle hollow site, and above the B–B bonds of the inner, middle, and outer rings. After structural relaxation, we found that the Li atom preferably is adsorbed above the central hexagonal vacancy at a distance of 1.60 Å with the maximum binding energy of $E_b = 1.88$ eV. The binding of Li to B_{36}^- is about 0.2 eV stronger. We further examined whether the Li binding energy changes on the N-doped clusters. When compared to the case of pristine B_{36}, the binding energy is significantly enhanced by $\sim$ 1.2–2.15 eV. As shown in Fig. 9, the maximum enhancement is observed in the case of Li

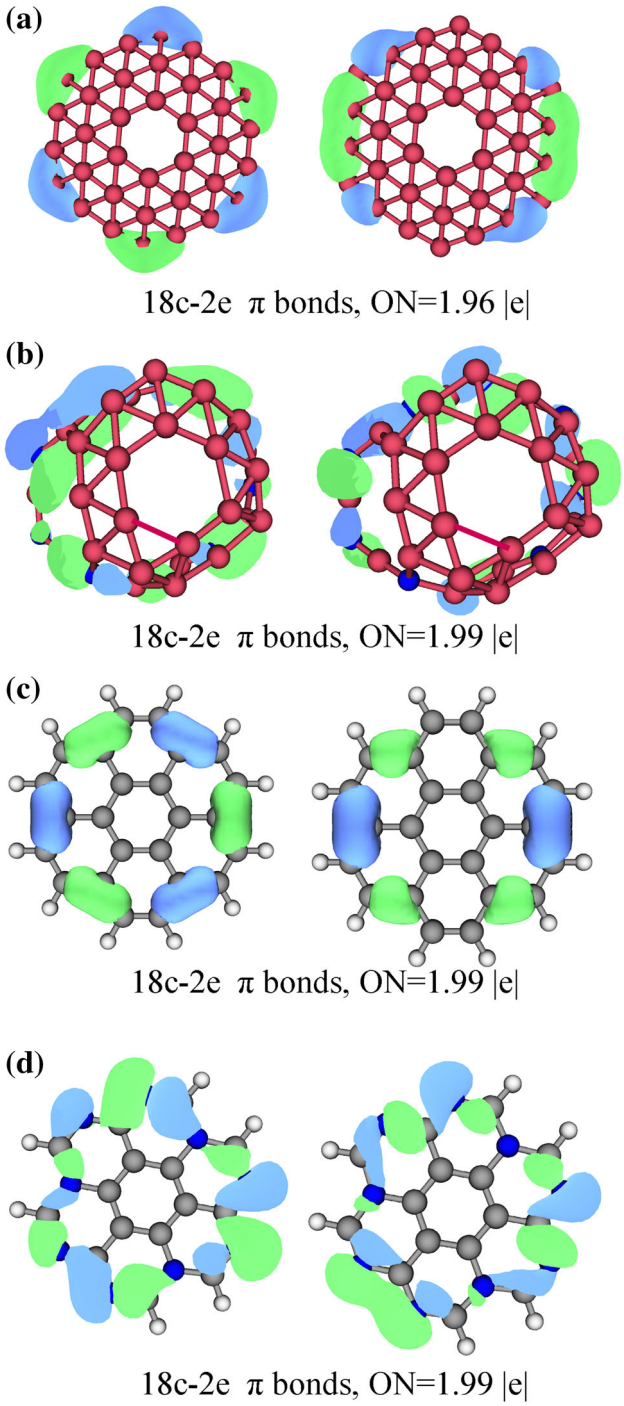

Figure 7 π bonding analysis using the AdNDP method for outer ring in **a** B_{36}, **b** $B_{27}N_9$, **c** $C_{24}H_{12}$, **d** $C_{15}N_9H_6$.

adsorption on $B_{33}N_3$. A similar trend has also been obtained for Li adsorption on anionic B_{36}^-. This finding suggests that different values of binding energies can be achieved by changing the charge state and introducing nitrogen into the B_{36} cluster. Moreover, the calculated binding energies are high enough to hinder clustering of alkali metals [47].

We also considered similar configuration for the adsorption of Na and K on the neutral and anionic B_{36} as well as their N-doped analogous. The trends in the binding energies are supported by the adsorption distance and the charge transfer between metal and substrates. The collected data in Table S2 show that the size of metal adatom and the dimension of the cavity on the boron cluster are two influential factors that determine the adsorption distance. In fact, the optimal distance ($d_{M\text{-substrate}}$) is determined by the repulsive forces between metal and the cluster. Hence, the largest distance belongs to the adsorption of K atom on $B_{30}N_6$ (having the smallest cavity size). Similar to the bonding mechanism of alkali metals on carbon surfaces [48], the adsorption of alkali metals on considered boron clusters is along with the electron transfer from metal to the cluster. The calculated natural charges of the metal center (Q_M) are summarized in Table S2. As might be anticipated, the magnitudes of charge transfer between alkali metals and $B_{33}N_3$ cluster are remarkably higher than those of other complexes.

This binding mechanism has also been confirmed by conducting the ELF analysis. The ELF theory is an important tool to study electronic structure and chemical bond analysis. Generally, a high value of ELF at a certain point is an indicator of the localized electrons therein. ELF is a dimensionless quantity that varies between 0 and 1. ELF = 0 corresponds to a completely delocalized situation, and ELF = 1 shows perfect localization; Fig. 10 presents the two-dimensional color-filled maps of Li adsorption on neutral B_{36} and three N-doped clusters. The left panel shows the ELF maps of bare clusters. In B_{36}, the high value of ELF (red color) in the outer ring indicates that the electrons are more likely confined in that region. Introducing nitrogen impurity reduces the degree of localization. In the case of $B_{27}N_9$, the map dominantly shows regions with ELF less than 0.4 implying delocalized features. In the adsorption systems (right panel) the quite low ELF, the blue area between Li and boron atoms of inner ring suggest weak interaction with electrostatic nature. It is interesting to note that the higher stability of Li/$B_{33}N_3$, as showed above by the binding energy, can also be demonstrated by the ELF map of the interacting system. The ELF in Fig. 10b indicates the large degree of

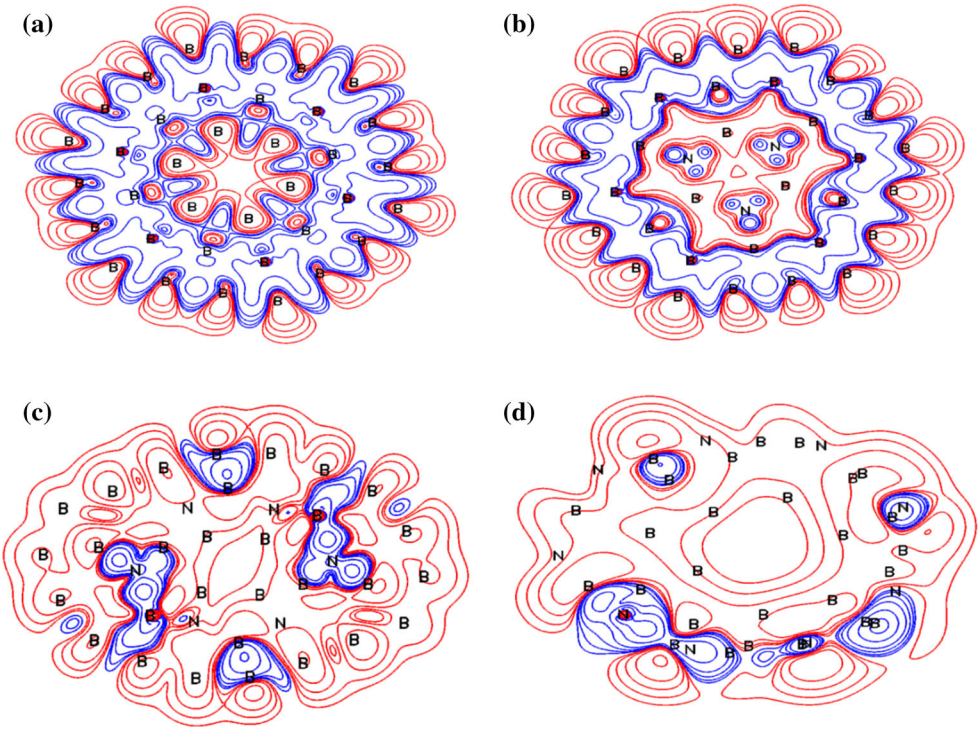

Figure 8 Contour maps of deformation electron density for **a** B_{36}, **b** $B_{33}N_3$, **c** $B_{30}N_6$, **d** $B_{27}N_9$. Positive and negative contours are represented by blue and red lines, respectively.

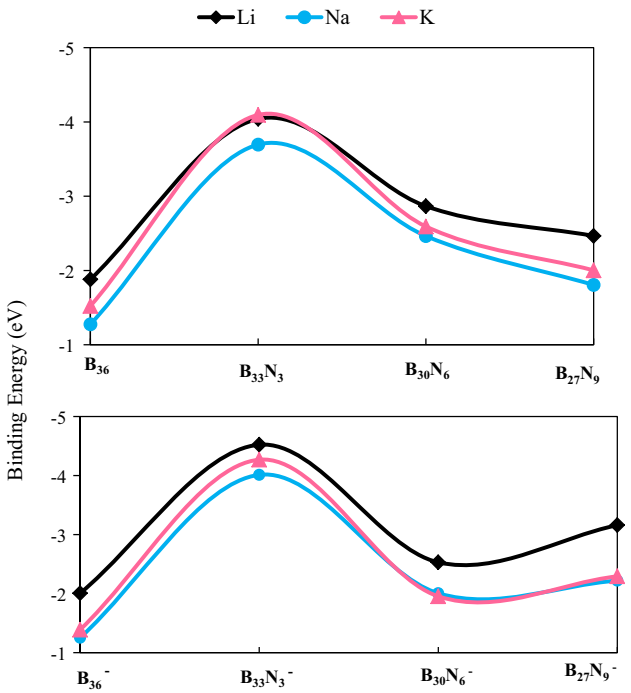

Figure 9 Binding energy variation of adsorbed metal on neutral (up) and anionic (down) substrates.

localization between boron atoms of the outer ring which is extended toward the middle ring in some region. In addition, the weak interaction between Li and boron atoms of the inner ring is also observed.

H_2 adsorption

We next study the adsorption of single hydrogen molecule on pristine and metallized substrates. Several initial configurations of the H_2 molecule including parallel and perpendicular to the hexagonal and triangle hollow sites as well as above the metal are examined. Upon relaxation, the hydrogen molecule prefers to locate above the central hexagonal hollow site in pristine and to tilt toward the metal in metallized substrates. The optimized structures of the hydrogen adsorption on the bare and metallized substrates are shown in Fig. 11, and the corresponding adsorption energies are presented in Fig. 12. The H_2 adsorption energy for pristine B_{36} is − 0.119 eV, and the adsorption distance is 3.50 Å. In the case of metallized B_{36}, the hydrogen molecule prefers to tilt toward alkali metal atoms so that one of the two H atoms becomes relatively closer to the metal atom. A summary of geometries related to the adsorption of H_2 on alkali metal decorated neutral and anionic B_{36} is given in Tables S3 and S4 in Supplementary

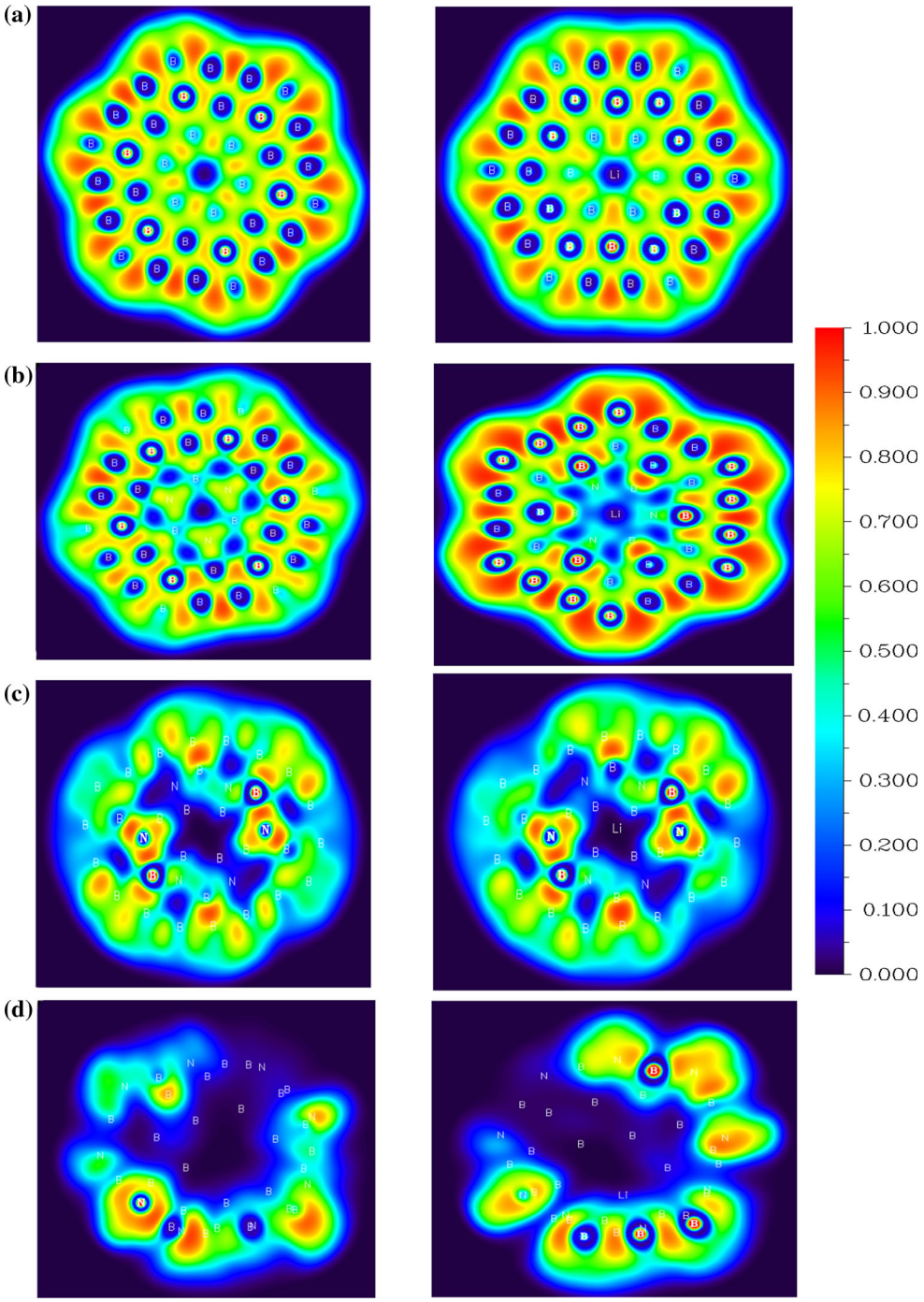

Figure 10 Color-filled maps of the ELF for the adsorption of Li on **a** B_{36}, **b** $B_{33}N_3$, **c** $B_{30}N_6$, and **d** $B_{27}N_9$. Left panel shows the bare clusters before Li adsorption. The values 0 (dark blue) and 1 (red color) correspond to a completely delocalized and perfect localized region, respectively.

Material. As shown in Fig. 12, metallization of B_{36} enhances the H_2 adsorption energies by 28–82%. The increase in the binding strength is in parallel with the decrease in the adsorption distance between metal and H_2. A similar trend has also been observed for the anionic B_{36} cluster.

Previous studies have demonstrated that N-doping decreases the adsorption energies of H_2 in carbon nanostructures [49, 50]. It is of our interest to know the effect of N-doping on the hydrogen adsorption behavior of B_{36}. Accordingly, we have systematically studied the adsorption behaviors of hydrogen molecules on N-doped B_{36}. For the sake of comparison, we considered similar adsorption configuration for N-doped clusters and their alkali metal coated forms. Inspection of Fig. 12 reveals that for $B_{33}N_3$, the H_2

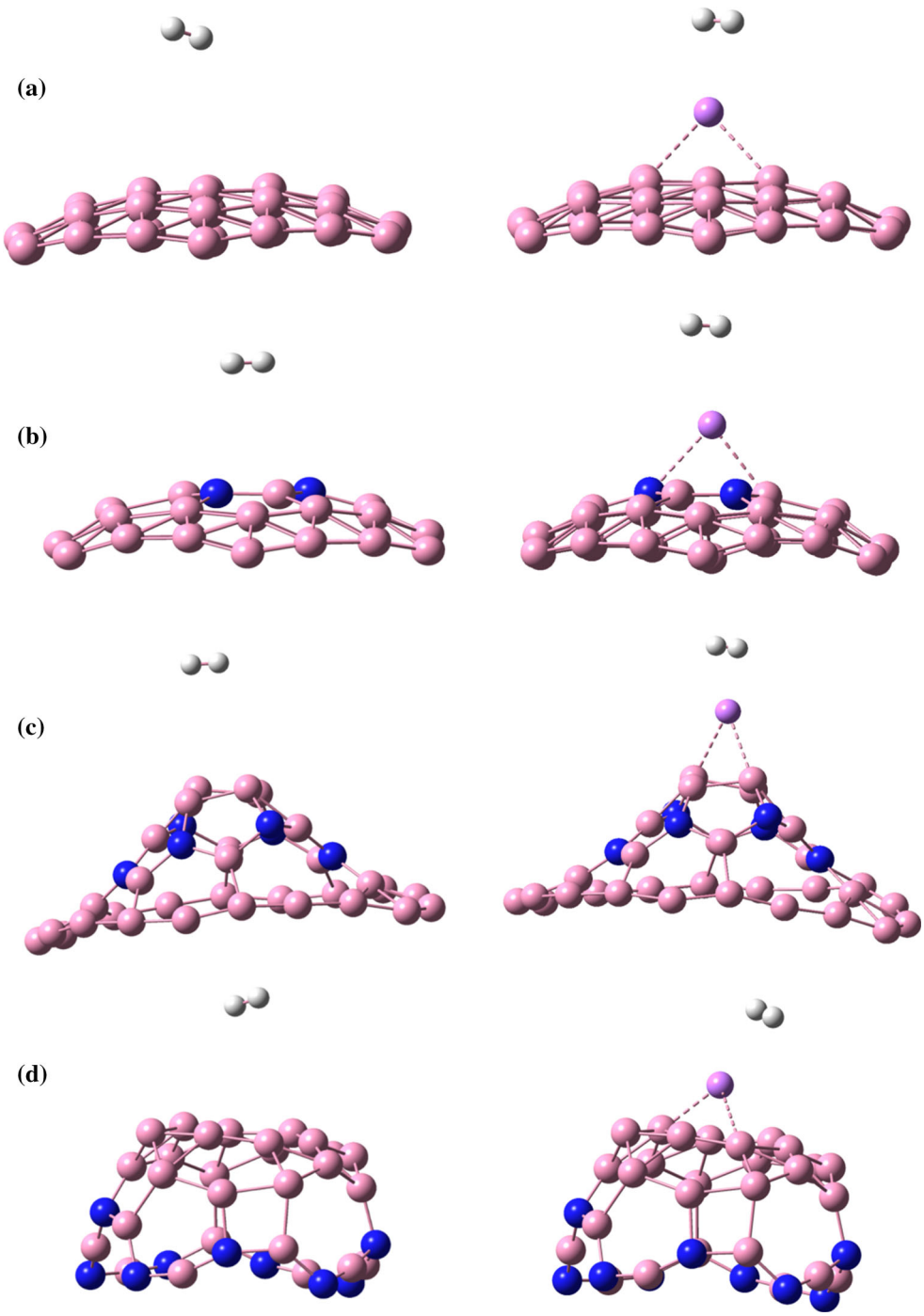

Figure 11 Optimized structure of hydrogen adsorption on bare (left) and metallized (right) substrates; **a** B_{36}, **b** $B_{33}N_3$, **c** $B_{30}N_6$, and **d** $B_{27}N_9$.

adsorption energy slightly increases as compared to B_{36}. At higher dopant concentration, a decrease in adsorption energy is observed. This result is in line with earlier reports for hydrogen adsorption of N-doped carbon materials. To obtain further understanding of H_2 adsorption mechanism, we have compared PDOS of an isolated hydrogen molecule with those of adsorbed H_2 on $B_{33}N_3$ and $Li/B_{33}N_3$ (Fig. 13). Isolated hydrogen molecule has two symmetric peaks at − 8 and 8 eV. After adsorption on $B_{33}N_3$, the PDOS of H_2 remains almost intact and a weak hybridization between H_2 and PDOS of nitrogen atoms is observed far below the Fermi level at − 9 to − 8 eV. In the case of $Li/B_{33}N_3$, the PDOS clearly reveals the charge transfer mechanism due to polarization interaction between H_2 and Li. The great

contribution of metal upon the H_2 adsorption is reflected by the obvious orbital interaction above the Fermi level at the region between 7 and 9 eV.

Conclusions

In conclusion, we have investigated the effect of nitrogen doping on the electronic structure and hydrogen adsorption properties of metallized B_{36} and B_{36}^- clusters. Three N-doped configurations resulted from N-doping at the inner, middle, and outer rings of B_{36} were considered. The structural features such as cluster curvature and size of the central hollow site have been systematically analyzed. Chemical bonding analysis of the doped clusters indicates the same analogy between concentric π bonding patterns of N-doped coronene and N-doped borophene. On the other hand, analysis of deformation electron density reveals that in the nitrogen-rich structures ($B_{30}N_6$ and $B_{27}N_9$ clusters), depletion of electron density results in the anisotropic distribution of electron density and cluster buckling.

We have also studied the adsorption of alkali metals on pristine and N-doped neutral and anionic B_{36} clusters. The binding energies of alkali metals depend on the curvature and nitrogen content of the substrate. Maximum binding strength is observed in the case of metallized $B_{33}N_3$. Further, we have reported the effect of N-doping on the hydrogen adsorption behavior of B_{36}. We showed that in $B_{33}N_3$, the H_2 adsorption energy slightly increases as

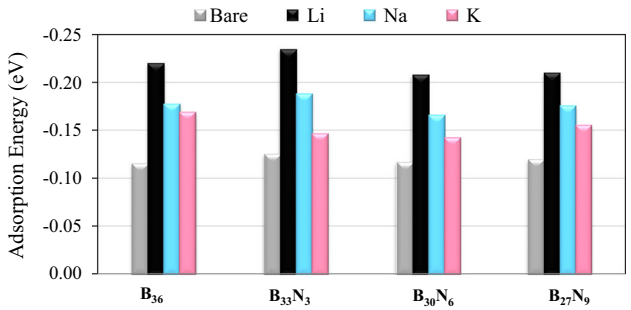

Figure 12 Adsorption energy of single hydrogen on bare and metallized substrates.

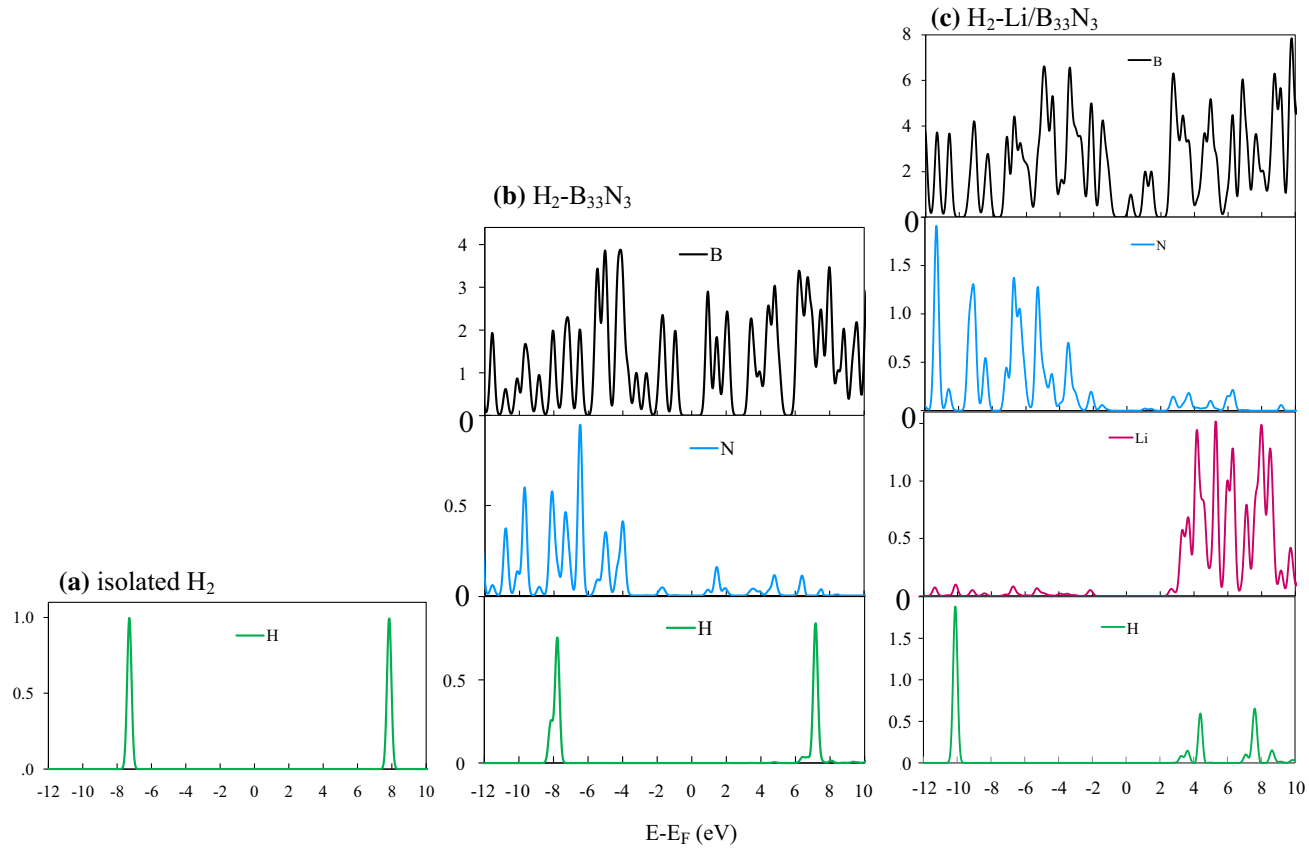

Figure 13 PDOS analysis of **a** an isolated hydrogen molecule, **b** H_2 adsorbed on $B_{33}N_3$, and **c** H_2 adsorbed on $Li/B_{33}N_3$.

compared to B_{36}, but at the higher level of dopant a decrease in adsorption energy is observed. However, depending on the type of metal and the nitrogen content, the H_2 adsorption energies vary in the range between − 0.11 and − 0.21 eV which lie in desirable range for reversible desorption near room temperature. We hope that our theoretical results will provide a useful guide for designing and synthesis of efficient hydrogen storage media.

Acknowledgements

This work is supported by the Shiraz University Research Council.

Compliance with ethical standards

Conflict of interest There is no conflict of interest regarding the publication of this article.

Electronic supplementary material: The online version of this article (https://doi.org/10.1007/s10853-017-1900-1) contains supplementary material, which is available to authorized users.

References

[1] Kiran B, Bulusu H, Zhai HJ, Yoo S, Zeng XC, Wang LS (2005) Planar-to-tubular structural transition in boron clusters: B_{20} as the embryo of single-walled boron nanotubes. Proc Natl Acad Sci USA 102:961–964

[2] Huang W, Sergeeva AP, Zhai HJ, Averkiev BB, Wang LS, Boldyrev AIA (2010) Concentric planar doubly π-aromatic B_{19}^- cluster. Nat Chem 2:202–206

[3] Popov IA, Piazza ZA, Li WL, Wang LS, Boldyrev AI (2013) A combined photoelectron spectroscopy and ab initio study of the quasi-planar B_{24}(-) cluster. J Chem Phys 139:144307-1–144307-8

[4] Oger E, Crawford NRM, Kelting R, Weis P, Kappes MM, Ahlrichs R (2007) Boron cluster cations: transition from planar to cylindrical structures. Angew Chem Int Ed 46:8503–8506

[5] Aihara JI, Kanno H, Ishida T (2005) Aromaticity of planar boron clusters confirmed. J Am Chem Soc 127: 13324–13330

[6] Liu CH, Wang X, Ye XJ, Yan X, Zeng Z (2014) Curvature and ionization-induced reversible hydrogen storage in metalized hexagonal B_{36}. J Chem Phys 141:194306-1–194306-8

[7] Mukherjee S, Thilagar P (2016) Borophene: a new paradigm! Curr Sci 111:1302–1304

[8] Mannix AJ, Zhou XF, Kiraly B, Wood J, Alducin DD, Myers BD, Liu X, Fisher BL, Santiago U, Guest JR et al (2015) Synthesis of borophenes: anisotropic, two-dimensional boron polymorphs. Science 350:1513–1516

[9] Sachdev H (2015) Disclosing boron's thinnest side. Science 350:1468–1469

[10] Tang H, Beigi S (2007) Novel precursors for boron nanotubes: the competition of two-center and three-center bonding in boron sheets. Phys Rev Lett 99:115501-1–115501-4

[11] Yang X, Ding Y, Ni J (2008) Ab initio prediction of stable boron sheets and boron nanotubes: structure, stability, and electronic properties. Phys Rev B 77:041402-1–041402-4

[12] Balendhran S, Walia S, Nili H, Sriam S, Bhaskaran M (2015) Elemental analogues of graphene: silicene, germanene, stanene, and phosphorene. Small 11:640–652

[13] Sachdev H, Muller F, Hufner S (2010) BN analogues of graphene: on the formation mechanism of boronitrene layers—solids with extreme structural anisotropy. Diamond Relat Mater 19:1027–1033

[14] Sergeeva PA, Popov IA, Piazza ZA, Li WL, Romanescu C, Wang L, Boldyrev AI (2014) Understanding boron through size-selected clusters: structure, chemical bonding, and fluxionality. Acc Chem Res 47:1349–1358

[15] Li S, Zhang Z, Long Z, Sun G, Qin S (2016) Comparative study on the spectral properties of boron clusters Bn0/−1(n = 38–40). Sci Rep 6:25020-1–25020-9

[16] Piazza ZA, Hu HS, Li WL, Zhao YF, Li J, Wang LS (2014) Planar hexagonal B_{36} as a potential basis for extended single-atom layer boron sheets. Nat Commun 5:3113-1–3113-6

[17] Li WL, Chen Q, Tian WJ, Bai H, Zhao YF, Hu HS, Zhai HJ, Li D, Wang LS (2014) The B_{35} cluster with a double-hexagonal vacancy: a new and more flexible structural motif for borophene. J Am Chem Soc 136:12257–12260

[18] Rastgou A, Soleymanabadi H, Bodaghi A (2017) DNA sequencing by borophene nanosheet via an electronic response: a theoretical study. Microelectron Eng 169:9–15

[19] Kootenaei A, Ansari G (2016) B_{36}. borophene as an electronic sensor for formaldehyde: quantum chemical analysis. Phys Lett A 380:2664–2668

[20] Jiang HR, Lu Z, Wu MC, Ciucci F, Zhao TS (2016) Borophene: a promising anode material offering high specific capacity and high rate capability for lithium-ion batteries. Nano Energy 23:97–104

[21] Zhang X, Hu J, Cheng Y, Yang H, Yau Y, Yang SA (2016) Borophene as an extremely high capacity electrode material for Li-ion and Na-ion batteries. Nanoscale 8:15340–15347

[22] Shi L, Zhao T, Xu A, Xu J (2016) Ab initio prediction of borophene as an extraordinary anode material exhibiting ultrafast directional sodium diffusion for sodium-based batteries. Sci Bull 61:1138–1144

[23] Zhao Y, Zeng S, Ni J (2016) Phonon-mediated superconductivity in borophenes. App Phys Lett 108:242601-1–242601-4

[24] Zhang Y, Wu ZF, Gao PF, Zhang S, Wen Y (2016) Could borophene be used as a promising anode material for high-performance li ion battery? ACS Appl Mater Interfaces 8:2175–22181

[25] Meng F, Chen X, Sun S, He J (2017) Electronic and magnetic properties of pristine and hydrogenated borophene nanoribbons. Phys E 91:106–112

[26] Ataca C, Akturk E, Ciraci S, Ustunel H (2008) High-capacity hydrogen storage by metallized graphene. Appl Phys Lett 93:043123–043125

[27] Kim D, Lee S, Hwang Y, Yun K, Chung Y (2014) hydrogen storage in li dispersed graphene with stone–wales defects: a first-principles study. Int J Hydrog Energy 39:13189–13194

[28] Yoon M, Yang S, Hicke C, Wang E, Geohegan D, Zhang Z (2008) Calcium as the superior coating metal in functionalization of carbon fullerenes for high-capacity hydrogen storage. Phys Rev Lett 100:206806–206809

[29] Chen C, Zhang J, Zhang B, Duan H (2013) Hydrogen adsorption of mg-doped graphene oxide: a first-principles study. J Phys Chem C 117:4337–4344

[30] Cabria I, Lopez MJ, Fraile S, Alonso J (2012) Adsorption and dissociation of molecular hydrogen on palladium clusters supported on graphene. J Phys Chem C 116:21179–21189

[31] Guo Y, Lan X, Cao J, Xu B, Xia Y, Yin J (2013) A comparative study of the reversible hydrogen storage behavior in several metal decorated graphyne. Int J Hydrog Energy 38:3987–3993

[32] Zhang H, Zhao M, Bu H, He X, Zhang M, Zhao L, Luo Y (2012) Ultra-high hydrogen storage capacity of li-decorated graphyne: a first-principles prediction. J Appl Phys 112:084305-1–084305-5

[33] Lu RF, Rao D, Meng Z, Zhang X, Xu G, Liu Y, Kan E, Xiao C, Deng K (2013) Boron-substituted graphyne as a versatile material with high storage capacities of Li and H_2: a multi-scale theoretical study. Phys Chem Chem Phys 15:16120–16126

[34] Wan W, Wang H (2015) First-principles investigation of adsorption and diffusion of ions on pristine, defective and B-doped graphene. Materials 8:6163–6178

[35] Rao D, Zhang L, Meng Z, Zhang X, Wang Y, Qiao G, Shen X, Liu J, Lu F (2017) Ultrahigh energy storage and ultrafast ion diffusion in borophene-based anodes for rechargeable metal ion batteries. J Mater Chem A 5:2328–2338

[36] Zhou J, Wang Q, Sun Q, Jena P, Chen XS (2010) Electric field enhanced hydrogen storage on polarizable materials substrates. Proc Natl Acad Sci USA 107:2801–2806

[37] Hussain T, Islam MS, Rao GS, Panigrahi P, Gupta D, Ahuja R (2015) Hydrogen storage properties of light metal adatoms (Li, Na) decorated fluorographene monolayer. Nanotechnology 26:275401-1–275401-6

[38] Li FY, Jin P, Jiang DE, Wang L, Zhang SB, Zhaoand JJ, Chen ZF (2012) B_{80} and $B_{101\text{-}103}$ clusters: remarkable stability of the core-shell structures established by validated density functionals. J Chem Phys 136:74302-1–074302-8

[39] Bai H, Chen Q, Miao C, Qmu YW, Wu YB, Lu GH, Zhai HJ, Li SD (2013) Ribbon aromaticity in double-chain planar B_nH_{22} − and $Li_2B_nH_2$ nanoribbon clusters up to n = 22: lithiated boron dihydride analogues of polyenes. Phys Chem Chem Phys 15:18872–18880

[40] Romanescu C, Harding DJ, Fielicke A, Wang LS (2012) Probing the structures of neutral boron clusters using infrared/vacuum ultraviolet two color ionization: B_{11}, B_{16}, and B_{17}. J Chem Phys 137:014317-1–014317-6

[41] Frisch MJ, Trucks GW, Schlegel HB, Scuseria GE, Robb MA, Cheeseman JR, Scalmani G, Barone V, Mennucci B, Petersson GA, et al (2013) Gaussian 09, revision D.01: Gaussian, Inc: Wallingford CT

[42] Zubarev DY, Boldyrev AI (2008) A developing paradigms of chemical bonding: adaptive natural density partitioning. Phys Chem Chem Phys 10:5207–5217

[43] Lu T Multiwfn, version 3.3.9. http://multiwfn.codeplex.com/

[44] Lu T, Chen F (2012) Multiwfn: a multifunctional wavefunction analyzer. J Comp Chem 33:580–592

[45] Chen Q, Wei GF, Tian WJ, Bai H, Liu ZP, Zhai HJ, Li SD (2014) Quasi-planar aromatic B_{36} and B_{36}^- clusters: all-boron analogues of coronene. Phys Chem Chem Phys 16:18282–18287

[46] Wang LS, Zhai HJ, Li SD, Li J, Boldy AI (2016) From planar boron clusters to borophene and borospherene. Proc of SPIE 10174:1017402-1–1017402-9

[47] Legrian F, Manzhos S (2015) Aluminum doping improves the energetics of lithium, sodium, and magnesium storage in silicon. J Power Sources 274:65–70

[48] Mohajeri A, Shahsavar A (2017) Tailoring the optoelectronic properties of graphyne and graphdiyne: nitrogen/sulfur dual doping versus oxygen containing functional groups. J Mater Sci 52:5366–5379

[49] Zhou Z, Gao X, Yan J, Song D (2006) Doping effects of B and N on hydrogen adsorption in single-walled carbon nanotubes through density functional calculations. Carbon 44:939–947

[50] Correa DJ, Florez F, Mora-Ramosb ME (2016) Ab initio study of hydrogen chemisorption in nitrogen-doped carbon nanotubes. Phys Chem Chem Phys 18:25663–25670